Direct Kinetic Determination of Rate Parameters for the Reaction CH₃ + OH. Implications for Methane Flame Modelling

R. Deters[1], H. Gg. Wagner[1], Á. Bencsura[2], K. Imrik[2], S. Dóbé[2*], T. Bérces[2], F. Márta[2],
F. Temps[3], T. Turányi[4], I. Gy. Zsély[4]

[1]Max-Planck-Institute für Strömungsforschung, Göttingen, Germany
[2]Chemical Research Center, Budapest, Hungary
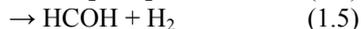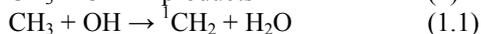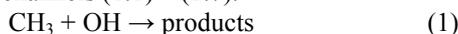[3]Institute für Physikalische Chemie, Universität Kiel, Kiel, Germany
[4]Department of Physical Chemistry, Eötvös University, Budapest, Hungary

Abstract

Kinetics of the overall reaction CH₃ + OH (1) were studied close to the high-pressure limit using the laser flash photolysis/transient UV absorption method (LFP/TAS) and in the fall-off regime with discharge flow/far infrared laser magnetic resonance (DF/LMR) at 298 K and 473 K, respectively. The product channel ¹CH₂ + H₂O (1.1) was also studied with the DF/LMR method. The following rate constants and branching ratio were determined (in He): k_1 (1463 mbar, 298 K) $\geq 6.2 \ 10^{13}$ cm³ mol⁻¹ s⁻¹, k_1 (1.16 mbar, 473 K) $\geq 5.2 \ 10^{13}$ cm³ mol⁻¹ s⁻¹ and $k_{1.1} / k_1 > 0.7$ (1.16 mbar, 473 K). Flame velocity for a standard CH₄-air flame was calculated in relation to the kinetics results.

1. Introduction

CH₃ and OH radicals occur in large concentration in the combustion of virtually all hydrocarbons. An understanding of their reactions with each other is crucial to the description of practical combustion systems, such as the natural-gas flame and internal combustion engines powered by fossil fuels. This reaction is of great interest also from a basic chemical kinetics point of view as being a multichannel radical-radical reaction which proceeds through formation and subsequent decomposition (or stabilisation) of vibrationally excited methanol intermediate (CH₃OH)*. According to its significance, many experimental [1 – 11] and theoretical [12 – 15] studies have been performed on the reaction CH₃ + OH in recent years. In spite of this extensive work, there are still considerable uncertainties in the kinetics and mechanism of this important and interesting reaction, concerning both the rate of the overall reaction (1) and, in particular, the efficiency of the different product channels (1.1) – (1.7).

$$CH_3 + OH \rightarrow products \quad (1)$$
$$CH_3 + OH \rightarrow {}^1CH_2 + H_2O \quad (1.1)$$
$$\rightarrow CH_3O + H \quad (1.2)$$
$$\rightarrow CH_2OH + H \quad (1.3)$$
$$\rightarrow {}^3CH_2 + H_2O \quad (1.4)$$
$$\rightarrow HCOH + H_2 \quad (1.5)$$
$$\rightarrow H_2CO + H_2 \quad (1.6)$$
$$CH_3 + OH + M \rightarrow CH_3OH + M \quad (1.7)$$

The energy diagram for reactions (1.1) – (1.7) is shown in Fig. 1. (The enthalpies of formation used are those given in [11] with the exception of the most recent revised values of $\Delta_f H°_{298}$ (OH) = 37.3 ± 0.3 kJ mol⁻¹ [16] and $\Delta_f H°_{298}$ (¹CH₂) = 428.1 ± 0.8 kJ mol⁻¹ [17].)

Fig. 1. Energy diagram for the reaction system CH₃ + OH.
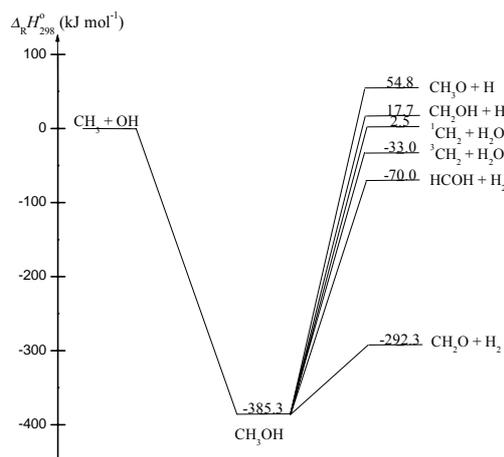
Among these reaction channels ¹CH₂ + H₂O (1.1) (see e.g. [10, 11]), CH₂OH + H (1.3) (see e.g. [12], [15]) and stabilisation to CH₃OH (1.7) (see e.g. [12]) have been suggested to play a major role under flame-relevant conditions, i.e. between about 800 and 2000 K and at normal pressures, with contribution from HCOH + H₂ (1.5) in the intermediate temperature regime [9]. A crucial question to flame modelling studies is the relative importance of the chain-propagating ¹CH₂ channel (1.1) compared to the chain-terminating recombination route (1.7). This question was subject to debate (see e.g. [4], [10, 11]), but a consensus appears to have been reached by recent studies [10, 11], [15]. These studies indicate that the reaction CH₃ + OH mostly acts as a chain-propagating step through the

---

dominance of channel (1.1) over channel (1.7) already at relatively low temperatures. It is to be noted, however, that $^1CH_2$ yield for $CH_3 + OH$ has been determined only in our own previous study [11] at room temperature. Also, no experimental data are available for the rate constant of the overall reaction in the pressure dependent region above room temperature. In a recent work [18], we have investigated the effect of the uncertainty of kinetic and thermodynamic data on methane flame simulation results. One of the main conclusions was that simulation results could be improved by better knowledge of the reaction rate parameters for the reaction $CH_3 + OH \rightarrow {}^1CH_2 + H_2O$ (1.1) at lean, stoichiometric and rich fuel-to-air ratios as well.

The objectives of the present study were the following: *(i)* determination of the overall rate constant, k_1, above ambient pressure at room temperature, *(ii)* determination of k_1 and the $^1CH_2$ branching ratio, $\Gamma = k_{1.1} / k_1$, in the low-pressure regime at 473 K, and *(iii)* calculation of laminar methane flame velocities in association with the kinetic results. Since the evaluation of the experimental data is still in progress, we present our preliminary results here.

Similarly to our previous investigation [11], two direct kinetic methods were used in the experiments that complement each other. The laser flash photolysis/transient UV absorption spectrometry apparatus (LFP/TAS) served to perform measurements at high pressures. The discharge flow/far infrared laser magnetic (DF/LMR) set-up was applied to investigate the kinetics of the reaction in the low pressure or fall-off region.

2. Experimental
2.1 LFP/TAS Experiments

The LFP/TAS apparatus is shown in Fig. 2. Unfocused 193 nm radiation of an ArF exciplex laser (Lambda Physik, Compex 201) was used as the photolysis source. The energy of the individual laser pulses was 360 ± 50 mJ with a few percent fluctuations between the subsequent laser pulses. The photolysis light was directed along the axis of a 50 cm long 5 cm inner diameter quartz reactor using a dielectric mirror (Laseroptik GmbH, HR 193-HT 200-400) placed in front of the reactor at a 45-degree angle. The second dielectric mirror that was placed behind the reactor prevented the laser beam to enter into the Xe lamp.

The overall flow of the gas mixture was typically 1 standard liter per minute. It contained the He buffer gas and the radical precursors, $CH_3C(O)CH_3$, N_2O and H_2O, in small concentration (< 0.004 %). All flows were regulated with needle valves (Hoke, Micromite) and the reactants' concentrations were obtained from the partial flows. The reaction pressure was measured with a 1000 Torr pressure transducer (MKS Baratron, 122A). The laser was operated at a 2/3 Hz repetition rate, which ensured complete replacement of the gas mixture in every 20 - 50 laser pulses depending on the experimental conditions.

CH_3 radicals were generated by the photolysis of acetone, $CH_3COCH_3 + h\nu$ (193 nm) $\rightarrow 2\ CH_3$ and OH radicals by the photolysis of nitrous oxide, and the subsequent reaction of the photolysis product singlet oxygen atom with water: $N_2O + h\nu$ (193 nm) $\rightarrow N_2 + O$ (^1D), followed by $O(^1D) + H_2O \rightarrow 2\ OH$.

An OH resonance lamp (2% H_2O/He, 150W microwave power) and a high-pressure Xe arc lamp (Osram, XBO 250W/4) were used as analytical light sources to monitor the OH and CH_3 radicals, respectively. The OH and CH_3 decays were taken in separate runs, but otherwise under identical experimental conditions. The light from the analysing lamps was focused by Suprasil lenses on the entrance slit of a 0.6 m monochromator (Jobin-Yvon, HR-640, 1200 gr/mm grating). OH radicals were detected around 308 nm with a 1-mm wide slit, resulting in an almost complete collection of the light from the A–X(0,0) electronic transition of OH. Prior to the kinetic experiments, a small wavelength region around 308 nm was scanned to find the emission maximum of the OH light source. The light from the OH lamp was reflected along the reactor axis by means of an Al mirror. The overlapping region of the laser beam and the analytical light beams was flushed with N_2 to avoid O_3 formation in front of the reactor.

CH_3 radicals were detected at 216.36 nm with the monochromator entrance slit set to 0.5 mm resulting in a 0.6 nm bandpass. The selected wavelength corresponds to the strong $\tilde{B} \leftarrow \tilde{X}$ transition of the CH_3 radical. Accurate calibration of the monochromator was periodically performed using the 253.65 nm emission line from a low-pressure Hg lamp. The spectrum of the Hg lamp was recorded between 250 – 260 nm using the Spectralink (Jobin-Yvon) stepping motor module interfaced to a PC. The accurate wavelength was identified as the maximum of the lamp profile by fitting a Gaussian curve to the measured spectrum. The analytical light beams leaving the monochromator were directed onto the photocatode of a UV-sensitive photomultiplier (EMI 9783R). The generated transient signals were captured in a digital storage oscilloscope (Tektronix, TDS40A, 500 MHz) and passed to a laboratory computer for averaging and further processing. An integrated hardware-software system (H-Interorg Ltd, Budapest) supplied the time variation of the OH and CH_3 absorbances from the measurements. Typically 500 decay traces were averaged to improve the signal-to-ratio. The absorption coefficient of the CH_3 radical was taken from McPerson et al. [19] to convert the methyl absorbances to concentrations.

Fig. 2. Schematic drawing of the laser flash photolysis/ transient UV absorption spectrometry apparatus (LFP/TAS)

DM: Dielectric mirror
DSO: Digital storage oscilloscope
AM: Al mirror
SM: Stepping motor
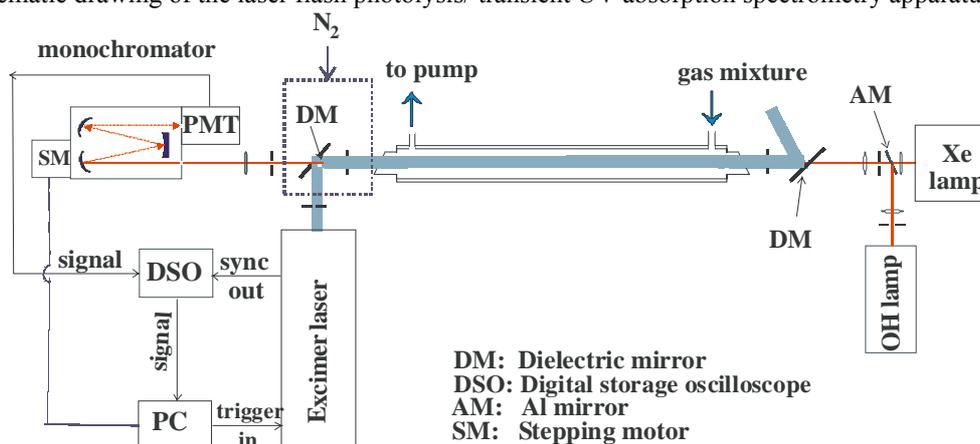
2.2 DF/LMR Experiments

A schematic diagram of the flow system used in this work is shown in Fig. 3. The flow reactor was made of quartz and had an internal diameter of 4.0 cm and overall length of 70 cm. Its inner surface was coated with a thin film of Teflon (Du Pont, FEP 856-200) in order to reduce the rate of heterogeneous wall reactions. The reactor was heated with an electric oven constructed specifically for the fast flow experiments (Fa. Horst, MQ 1057). Along the effective reaction distance of 50-cm, the temperature deviation from the mean 473 K did not exceed ± 3 K as measured directly within the gas stream with a calibrated thermocouple. The reaction pressure was measured at the downstream end of the reactor in the LMR absorption cell by using a capacitance manometer (MKS Baratron, 10 Torr head).

Fig. 3. Schematic drawing of the isothermal fast discharge flow apparatus (DF)
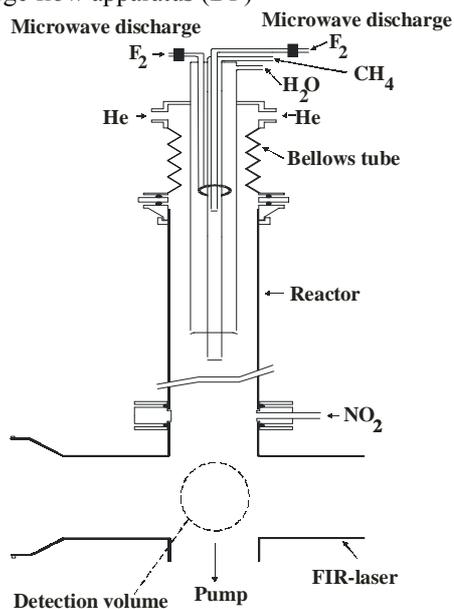

Time resolution was achieved with a moveable quartz injector of 2.8 cm o. d. which was mounted co-axially to the upper end of the reactor using a large bore diameter bellows tube. CH_3 and OH radicals were produced inside the injector by the spatially separated reactions $F + CH_4 \rightarrow CH_3 + HF$ and $F + H_2O \rightarrow OH + HF$. The injector probe shown in Fig. 3 allowed us to control the CH_3 and OH concentrations independently from each other, moreover, this arrangement had the advantage of providing constant $[CH_3]_0$ and $[OH]_0$ at each reaction distance. Fluorine atoms were generated at the upper end of the injector by flowing dilute F_2/He mixtures through alumina-lined discharges excited by 2450 MHz microwave generators (Bosch, Radamed and Medical Supplies, Microtron 200).

The flow tube was coupled to a FIR-LMR spectrometer, a schematic drawing of which is presented in Fig. 4. A detailed description of the spectrometer can be found in [20]. The FIR laser was optically pumped in the transverse mode with a CO_2 laser (Laser Photonics, Model 575). It provides a few thousand lines in the wavelength region between about 40 μm and 2 mm. The LMR sample region was located intracavity between the pole caps of a 15'' electromagnet (Bruker). The LMR absorption signals were detected with a liquid helium cooled Si bolometer (Infrared Laboratories), processed in a lock-in amplifier (EG&G Brookdeal, SC9505), recorded on a strip-chart recorder and digitised for further analysis in a laboratory PC.

The FIR-LMR detection parameters are given in ref. 11. $^1CH_2$ was monitored in its ground-state triplet form, $^3CH_2$, providing an excellent LMR sensitivity. Detection of CH_3 radicals was achieved in the form of NO via the fast conversion reaction of CH_3 with NO_2 carried-out directly in the sample cell of the spectrometer. Determination of Γ required the knowledge of absolute concentrations for CH_3, OH and CH_2. These were obtained by daily calibrations, using the gas-titration reactions, $CH_3 + NO_2 \rightarrow CH_3O + NO$, $H + NO_2 \rightarrow OH + NO$ and $O + CH_2CO \rightarrow CH_2 + CO_2$, respectively [11].

Fig. 4. Schematics of the CO_2 laser pumped far infrared laser magnetic resonance spectrometer (LMR)
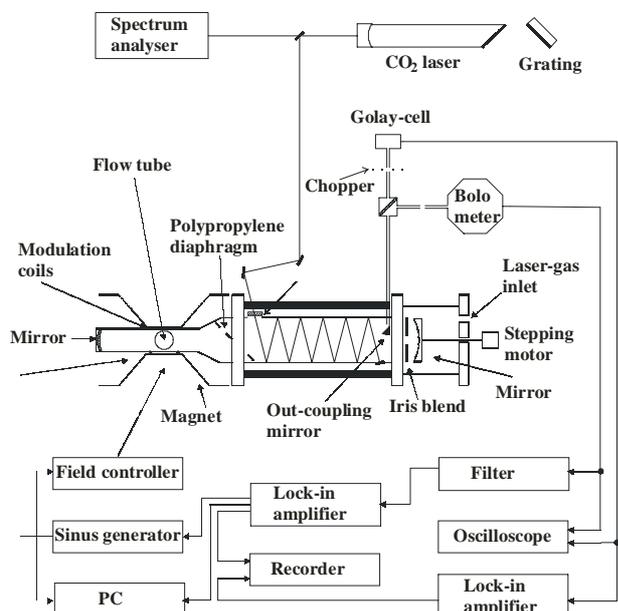
Helium was the carrier gas. The main gas flows were regulated and monitored by calibrated mass flow controllers (Tylan, FC-260). The smaller flow rates were set by stainless-steel needle valves (Hoke, Micromite) and determined by measuring the change in pressure versus time of gas flows into standard volumes. H_2O was vaporised into a He flow in a two-stage saturator thermostated slightly below room temperature. Materials used in the experiments are listed in Table1.

Table 1
Gases and chemicals used in the LFP/TAS and DF/LMR experiments

Name	Origin	Purity (%)	Notes
He	Messer-Griesheim	99.9990	a
	Messer-Griesheim	99.9999	b
H_2	Messer-Griesheim	99.9990	b
F_2	Messer-Griesheim	99.995	b
O_2	Messer-Griesheim	99.998	b
NO	Messer-Griesheim	≥99	b, c
N_2O	Union Carbide	99.998	a
NO_2	Messer-Griesheim	≥ 99	a, b, c
H_2O	Double distilled		a, b, d
CH_4	Messer-Griesheim	99.995	b
Acetone	Aldrich	> 99.9	a, d
CH_2CO	Own synthesis	≥ 98	b, e

[a] LFP/TAS experiments. [b] DF/LMR experiments. [c] Purified by low-temperature distillation. [d] Degassed prior to use. [e] Obtained by pyrolysis of acetone on Ni/Cr wires at $T ≈ 900$ K and purified by low-temperature distillation.
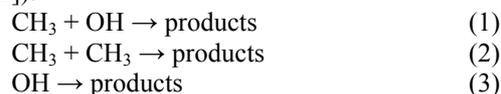
3. Results and Discussion
3.1 Kinetics of the Reaction $CH_3 + OH$

The following experimental conditions were applied in this study:
LFP/TAS: $T = 298 ± 2$ K, $P = 1463$ mbar, $[CH_3(CO)CH_3] = 2.5 \ 10^{-9}$ mol cm^{-3}, $[N_2O] = 1.8 \ 10^{-8}$ mol cm^{-3} and $[H_2O] = 9.2 \ 10^{-10}$ mol cm^{-3}; DF/LMR: $T = 473 ± 3$ K, $P = 1.16$ mbar, $[F_2]_0 = 9.6 \ 10^{-12}$ mol cm^{-3}, $[H_2O] = 2.4 \ 10^{-10}$ mol cm^{-3} and $[CH_4] = 4.2 \ 10^{-10}$ mol cm^{-3}. In both types of experiments CH_3 was at least in tenfold excess over OH.

Overall kinetics. Determination of k_1 required the simultaneous monitoring of the time history of both the CH_3 and OH radicals. The depletion of the excess component methyl obeyed second order kinetics, as it is seen by the plot of $1 / [CH_3]$ vs. reaction time presented in Fig 6b. The decay of OH radicals was ruled essentially by reaction (1) and could be described by the simple reaction mechanism (1) – (3) and the corresponding kinetic expression, Eq. (I) (see also [6], [10, 11]):

$$CH_3 + OH \rightarrow products \qquad (1)$$
$$CH_3 + CH_3 \rightarrow products \qquad (2)$$
$$OH \rightarrow products \qquad (3)$$

$$[OH] = [OH]_0 \, (1 + 2k_2 [CH_3]_0 \, t)^{-k_1 / 2k_2} \exp(-k_3 t) \quad (I)$$

Reaction (3) is predominantly the pseudo-first-order reaction with acetone and the heterogeneous wall loss of OH in the LFP/TAS and DF/LMR systems, respectively. These reactions could be determined in separate experiments. Typical fitting plots are shown in Figs. 5 and 6a. The results, along with those obtained previously [11], are summarized in Table 2. The kinetic data from the current work are reported as lower limits in Table 2. This is because computer simulations with more detailed reaction mechanisms are still underway and the final results are expected to be slightly larger.

Fig. 5. OH decay plots for the determination of k_1 in a representative DF/LMR experiment at $T = 475$ K and $P = 1.16$ mbar ($[CH_3]_0 = 1.12 \ 10^{-12}$ mol cm^{-3}, $[CH_3]_0 / [OH]_0 ≈ 11$)
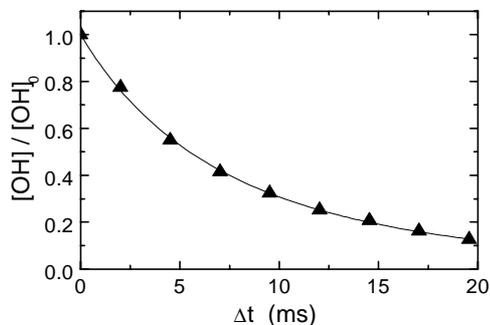
Fig. 6. OH and CH_3 decay plots for the determination of k_1 in a representative LFP/TAS experiment at $T = 298$ K and $P = 1463$ mbar ($[CH_3]_0 = 2.05 \ 10^{-10}$ mol cm^{-3}, $[CH_3]_0 / [OH]_0 \approx 12$).
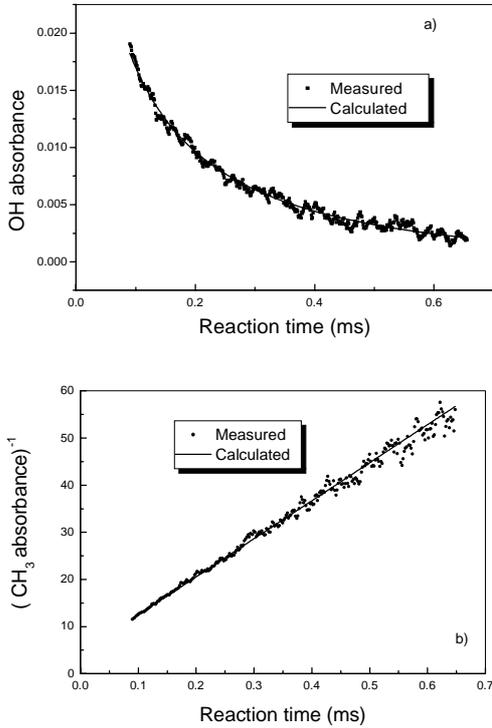

Table 2
Summary of the experimental results (all pressures refer to $T = 298$ K, He puffer gas)

T (K)	P (mbar)	$10^{-13} \ k_1 \ (\pm 2\sigma)$ (cm^3 mol^{-1} s^{-1})	$\Gamma = k_{1.1} / k_1$	Notes
298 ± 2	0.73	3.0 ± 0.4		a, b
	1.33	3.2 ± 0.4	0.89 ± 0.09	a, b
	$45 - 467$	4.4 ± 0.8		a, b
	1463	$\geq 6.2 \ (25)^e$		c, d
473 ± 3	0.73	$\geq 5.2 \ (5)^e$		b, d
473 ± 3	0.73		$> 0.7 \ (5)^e$	b, d

^{a}Taken from [11]. ^{b}DF/LMR technique. ^{c}LFP/TAS technique. ^{d}This work. ^{e}Number of experiments.

Evaluation of the LFP/TAS experimental data according to Eq. (I), returned $k_1 \geq 6.2 \ 10^{13}$ cm^3 mol^{-1} s^{-1} at $T = 298$ K and $P = 1463$ mbar He pressure. Our previous high-pressure rate constant is about 30% smaller [11] (see in Table 2). This deviation can be attributed to the slight residual pressure dependence of the reaction beyond 467 mbar, the highest pressure in [11]. The new larger k_1 value is in excellent agreement with the limiting high-pressure rate constant of $k_{1 \ (\infty)}$ (298 K) = 6.0 10^{13} cm^3 mol^{-1} s^{-1} recommended by the CEC critical data evaluation [25].

The low-pressure DF/LMR measurements have supplied the overall rate constant value of $k_1 \geq 5.2 \ 10^{13}$ cm^3 mol^{-1} s^{-1} at $T = 473$ K and $P = 1.16$ mbar He pressure. That is, similarly to our room temperature findings [11] (see in Table 2), a very small pressure dependence could be observed only. The low-pressure

rate constant increases slightly with temperature. These observed P and T dependencies show just the opposite behaviour one would expect if only the association product CH_3OH was formed in the reaction of CH_3 with OH.

$^1CH_2$ formation. Methylene formation was studied in the low-pressure experiments with the DF/LMR apparatus at $T = 473$ K and $P = 1.16$ mbar He pressure. Similarly to our observations at room temperature [11], large triplet methylene signals were detected in the experiments. It was attributed to the occurrence of reaction (1.1) and the subsequent fast collision induced intersystem crossing process, $^1CH_2 + M \rightarrow {}^3CH_2 + M$, which was complete on a very short time-scale in the reaction system. An alternative, direct $^3CH_2$ formation on a triplet potential energy surface, $CH_3 + OH \rightarrow {}^3CH_2 + H_2O$ (1.4), is much less probable because of the high barrier of this latter reaction [14, 15]. Determination of $\Gamma = k_{1..1} / k_1$ required the measurement of the time variation of $[CH_3]$, $[OH]$ and $[^3CH_2]$. Typical OH and $^3CH_2$ concentration profiles are presented in Fig. 7.

Fig. 7. OH and CH_2 concentrations as a function of reaction time in a representative DF/LMR experiment designed to obtain $\Gamma = k_{1.1} / k_1$ ($T = 475$ K, $P = 1.16$ mbar $[CH_3]_0 = 1.57 \ 10^{-12}$ mol cm^{-3}, $[CH_3]_0 / [OH]_0 \approx 10$)
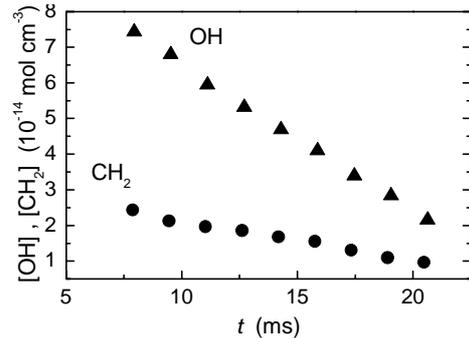
As it is seen in Fig. 7, the $^3CH_2$ radicals are consumed in the reaction already at the shortest reaction time that was accessible by the DF technique. This is a consequence of the occurrence of fast secondary reactions, among which $^3CH_2 + OH$ and $^3CH_2 + CH_3$ are the most important. Thus, the branching ratio can be obtained via computer simulations only. The first computations have revealed that $^1CH_2 + H_2O$ are the main reaction products and that it is safe to propose a definite lower limit from the present study. This is given as $\Gamma = k_{1.1} / k_1 > 0.7$ ($T = 473$ K, $P = 1.16$ mbar).

The high $^1CH_2$ branching ratios obtained in the low pressure investigations, in [11] and this work, indicate that the reaction channel $CH_3 + OH \rightarrow {}^1CH_2 + H_2O$ (1.1) will be important under flame relevant conditions as well leading to chain propagation in contrast to the chain terminating combination to CH_3OH. This view has been supported by a recent ILT/ME theoretical study by Pilling and co-workers [10] and the ab initio/VRRKM computations by Lin and co-workers. These theoretical works provide the possibility to guide

the extrapolation of the kinetic data to combustion conditions.

3.2 Methane Flame Modelling

Computer simulations were carried out to calculate flame velocities for premixed, adiabatic, one-dimensional methane-air flames using the PREMIX code [21] of the CHEMKIN-II program suite [22]. The chemical mechanism applied was the Leeds Methane Oxidation Mechanism [23] in its latest version 1.5 (abbreviated here as LM1.5). LM1.5 contains 37 species and 175 reversible reactions; the commented mechanism can be downloaded from the web [24]. In LM1.5, the multichannel reaction $CH_3 + OH$ has been taken into account by recommendations from the CEC evaluation [25] and in a great part by our own laboratory kinetic results [11], [26] (see also the comments in [24]). Our previous results have been confirmed and extended by the experimental determinations in the current study.

The calculated laminar flame velocity is plotted in Fig. 8, together with two more recent experimental data sets [27, 28]. The unburned gas temperature was 298 K and the pressure 1.0 atmosphere. The agreement between the experimental data and the calculations is seen to be reasonable, but the deviation becomes larger in the rich mixtures. This may indicate deficiencies in the mechanism concerning the reactions of the larger molecular-weight species. We note that this is the first reported validation of LM1.5 in calculating methane flame velocities.

Fig. 8. Flame velocity as a function of equivalence ratio for a methane-air mixture. T_u = 298 K. ○ - Vagelopoulos et al. [27], ● - Taylor [28].
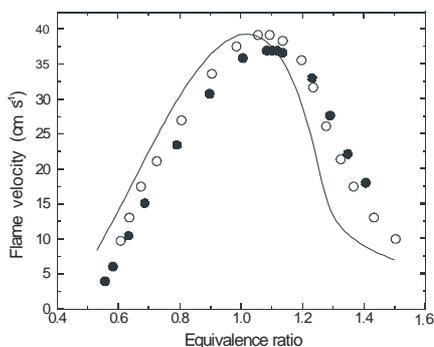
References

[1] T.Sworski, C.J. Hochenadel, P.J. Ogren, J. Phys. Chem. 84 (1989) 129-134.

[2] C. Anastasi, P. Ellermann, P. Pagsberg, S.J. Polak, J. Chem. Soc. Faraday Trans. 87 (1991) 2325-2328.

[3] J.F. Bott, N Cohen, Int. J. Chem. Kinet. 23 (1991) 1017-1033.

[4] H. Oser, N.D. Stothard, R. Humpfer, H.H. Grotheer, J. Phys. Chem. 96 (1992) 5359-5363.

[5] H. Oser, N.D. Stothard, R. Humpfer, H.H. Grotheer, Th. Just, 24th Symp. (Int.) Combust. (1992) 597-604.

[6] K.J. Hughes, R.A. Pereira, M.J. Pilling, Ber. Bunsenges. Phys. Chem. 92 (1992) 1352-1359.

[7] K. Fagerström, A. Lund, G. Mahmoud, J.T. Jodkowski, E. Ratajczak, Chem. Phys. Lett. 204 (1993) 226-234.

[8] K. Fagerström, A. Lund, G. Mahmoud, J.T. Jodkowski, E. Ratajczak, Chem. Phys. Lett. 224 (1994) 43-50.

[9] R. Humpfer, H. Oser, H.-H. Grotheer, Th. Just, 25th Symp. (Int.) Combust. (1994) 721-731.

[10] R.A. Pereira, D.L. Baulch, M.J. Pilling, S.H. Robertson, G. Zeng, J. Phys. Chem. A 101 (1997) 9681-9693.

[11] R. Deters, M. Otting, H.Gg. Wagner, F. Temps, B. László, S. Dóbé, T. Bérces, Ber. Bunsenges. Phys. Chem., 102 (1998) 58-72.

[12] A.M. Dean, P.M. Westmoreland, Int. J. Chem. Kinet. 19 (1987) 207-216.

[13] S.P. Walch, J. Chem. Phys. 98 (1993) 3163-3167.

[14] C. Wilson, G.G. Bálint-Kürti, J. Phys. Chem. A, 102 (1998) 1625-1631.

[15] W.S. Xia, R.S. Zhu, M.C. Lin, A.M. Mebel, Faraday Discuss., 119 (2001) 191-205.

[16] B. Ruscic, A.F. Wagner, L.B. Harding, R.L. Asher, D. Feller, D.A. Dixon, K.A. Peterson, Y. Song, X. Qian, C.Y. Ng, J. Liu, W. Chen, D.W. Schwenke J. Phys. Chem. A, 106 (2002) 2727-2747.

[17] B. Ruscic, M. Litorja, R.L. Asher J. Phys. Chem. A, 106 (1999) 8625-8633.

[18] T. Turányi, L. Zalotai, S. Dóbé, T. Bérces, Phys. Chem. Chem. Phys., 4 (2002) 2568-2578.

[19] M.T. Macperson, M.J. Pilling, M.J.C. Smith, J. Phys. Chem., 89 (1985) 2268-2276.

[20] T. Böhland, F. Temps, H.Gg. Wagner, Z. Phys. Chem., Neue Folge, 142 (1986) 129.

[21] Kee, R.J., J.F. Grcar, M.D. Smooke, J.A. Miller, *A Fortran Program for Modeling Steady Laminar One-Dimensional Premixed Flames*, Sandia National Laboratories Report No. SAND85-8240, 1985.

[22] R.J. Kee; F.M. Rupley; J.A. Miller, *Chemkin-II: A Fortran Chemical Kinetics Package for the Analysis of Gas Phase Chemical Kinetics*, Sandia National Laboratories Report No. SAND89-8009B, 1991.

[23] K.J. Hughes, T. Turányi, A.R. Clague, M.J. Pilling, Int. J. Chem. Kinet., 33 (2001) 513.

[24] M.J. Pilling, T. Turányi, K.J. Hughes, http://www.chem.leeds.ac.uk/Combustion/

[25] D.L. Baulch, et al, Combust. Flame, 98 (1994) 59-79.

[26] S. Dóbé, T. Bérces, F. Temps, H.Gg. Wagner, H. Ziemer, J. Phys. Chem., 98 (1994) 9792-9800.

[27] C.M. Vagelopoulos, F.N. Egolfopoulos, C.K. Law, 25th Symp (Int) on Combustion, The Combustion Institute: Pittsburgh, 1994, 1341-1347.

[28] S.C. Taylor, Ph.D. thesis, University of Leeds, 1991.